Mirror and Firehose Instabilities in the Heliosheath

Vincent Génot

Mirror and firehose instabilities in the heliosheath

V. Génot

CESR/CNRS, Université Paul Sabatier, Toulouse, France

vincent.genot@cesr.fr

ABSTRACT

We investigate the nature of the heliosheath plasma behind the Termination Shock across which jump relations in anisotropic MHD are formulated. Along side analytical results for downstream parameters in the strictly parallel and perpendicular cases we numerically solve the Rankine-Hugoniot relations for arbitrary shock angle and strength. We then focus on two temperature anisotropy driven instabilities which have attracted attention in many other astrophysical situations, namely the mirror and firehose instabilities. It is revealed that the firehose instability is mainly controlled by the shock strength with little influence of the shock angle contrary to the mirror instability for which both parameters intervene. We confirm results showing that the heliosheath plasma observed by Voyager 1 immediately behind the Termination Shock is mirror unstable. Similar conditions are probable in the heliosheath recently encountered by Voyager 2. Finally, by comparison with studies in the Earth's magnetosheath context, we formulate predictions on the shapes of mirror associated magnetic fluctuations in the heliosheath. Both hole and peak magnetic structures were indeed observed by Voyager 1 and these shapes correspond to different stages of the mirror instability.

Subject headings: solar wind, shock waves, plasmas, MHD, instabilities, methods: numerical

1. Introduction

Recent in-situ measurements in the heliosheath have paved the way for comparative studies with planetary magnetosheaths whose characteristics are scrutinized for many years. Among these studies the plasma turbulence induced by shocks is one of the favorite. Indeed shocks are efficient machine to produce temperature anisotropy, i.e. particle distribution functions observed downstream of shocks are anisotropic with respect to the background

magnetic field. This anisotropy is a free energy which is consumed by various instabilities depending on the plasma β. Mirror mode will grow unstable in sufficiently high β plasma for $T_\perp/T_\parallel > 1$, whereas the firehose instability will develop for $T_\perp/T_\parallel < 1$ where T is the temperature and subscripts $\perp$ and $\parallel$ refer to the direction perpendicular and parallel to the ambiant magnetic field respectively. Observationally mirror associated fluctuations have been reported in different astrophysical contexts : the Earth (Génot et al. 2008a), Jupiter (Joy et al. 2006), Saturn (Bavassano Cattaneo et al. 1998), the Io wake (Huddleston et al. 1999), the comet Halley (Russell et al. 1987), the solar wind (Winterhalter et al. 1994), in front of Interplanetary Coronal Mass Ejection (Liu et al. 2006), in the heliosheath (Burlaga et al. 2006) and probably in galaxy clusters (Schekochihin et al. 2008).

On the contrary firehose associated fluctuations have been rarely reported in planetary magnetosheaths. Indeed global magnetospheric MHD simulations (Erickson et al. 2002) have shown that firehose unstable regions are very localized. Such regions are however a common feature of solar wind observations (Kasper et al. 2002) and, in the heliosheath environnement, observations of firehose instability are envisageable.

The recent in-situ measurements by Voyager 1 (V1) upstream and downstream of the Termination Shock (TS) fueled analysis which revealed that mirror instability is certainly at work in the heliosheath plasma (Burlaga et al. 2006; Liu et al. 2007). The shock crossed by V1 (hereafter TS1) was perpendicular which is implied, on average, by the tight winding of the Archimedes spiral magnetic field at large heliocentric radial distances. However other orientations may be expected especially in the downwind direction of the heliopshere where it is elongated by its interaction with the interstellar wind. Indeed recent observations by Voyager 2 (V2) (Stone et al. 2008) support the view of an asymmetric heliopshere, and the third TS crossing by V2 (hereafter TS3) is an oblique shock (Richardson et al. 2008). In this context, the purpose of the present paper is to propose a general procedure which addresses the question of the nature of the heliosheath plasma behind varied TS conditions characterized in term of shock angle and strength. We shall adopt an anisotropic MHD formalism keeping in mind that recent kinetic developments may be more rigorous to analyze the fine structure of the shock transition (Fahr and Siewert 2007; Siewert and Fahr 2008). In the next section we present and analytically and numerically solve the jump relations used to compute the downstream anisotropy and plasma β which are required to express instability thresholds. In Section 3 we discuss our results in the light of V1 and V2 measurements and in Section 4 predictions following an analogy with mirror mode studies in the Earth's magnetosheath context are presented.

2. Resolution of the jump conditions at the Termination Shock

In the following we basically follow the same approach than Liu et al. (2007). Considering a bi-Maxwellian plasma, the jump relations across a shock are Hudson (1970) :

$$[B_n] = 0 \tag{1}$$

$$[\rho v_n] = 0 \tag{2}$$

$$[v_n \vec{B}_t - \vec{v}_t B_n] = 0 \tag{3}$$

$$\left[P_\perp + \left(P_\parallel - P_\perp\right)\frac{B_n^2}{B^2} + \frac{B_t^2}{2\mu_0} + \rho v_n^2\right] = 0 \tag{4}$$

$$\left[\frac{B_n \vec{B}_t}{\mu_0}\left(\frac{P_\parallel - P_\perp}{B^2/\mu_0} - 1\right) + \rho v_n \vec{v}_t\right] = 0 \tag{5}$$

$$\left[\rho v_n \left(\frac{2P_\perp}{\rho} + \frac{P_\parallel}{2\rho} + \frac{v^2}{2} + \frac{B_t^2}{\mu_0 \rho}\right) + \frac{B_n^2 v_n}{B^2}\left(P_\parallel - P_\perp\right) - \frac{(\vec{B}_t \cdot \vec{v}_t)B_n}{\mu_0}\left(1 - \frac{P_\parallel - P_\perp}{B^2/\mu_0}\right)\right] = 0 \tag{6}$$

The square brackets indicate the difference between pre-shock (upstream) and post-shock (downstream) states, μ_0 is the permeability of the vacuum, k is the Boltzmann constant, ρ is the plasma density, $\vec{v}$ and $\vec{B}$ are the plasma velocity and magnetic field vectors respectively, $P = \rho kT/m$ is the plasma pressure, and m the proton mass; subscripts t and n denote the tangential and normal components with respect to the shock surface, and subscripts 1 and 2 in the following correspond to upstream and downstream states respectively. The velocity is measured in the shock frame and we assume that the bulk velocity is parallel to the shock normal ($v_{t1} = 0$) which is consistent with the TS being close to a spherical surface. The shock angle θ_{Bn} is the angle between the shock normal and the Interplanetary Magnetic field at the shock, and the shock strength (or density compression ratio) r_s is defined by :

$$r_s = \frac{\rho_2}{\rho_1} \tag{7}$$

It can be expressed in term of normal velocities using Equation 2 and, in the case of a perpendicular shock only, is also equal to $\frac{B_2}{B_1}$. We also define the temperature anisotropy by $A = T_\perp/T_\parallel$, the upstream Alfvén Mach number $M_{A1}^2 = \mu_0\rho_1 v_1^2/B_1^2$ and $\beta_1 = 2\mu_0 P_1/B_1^2$.

The system of equations above is under determined (6 equations, 7 unknowns $= v_{n2}, v_{t2}, B_{n2}$, $B_{t2}, P_{\parallel 2}$ or $\beta_{\parallel 2}, A_2, \rho_2$) therefore solving it requires an extra information like an equation of state or a marginal stability equation (Chao et al. 1995; Vogl et al. 2001). Our approach here is different : after eliminating three quantities (v_{n2}, v_{t2}, B_{n2}) we keep ρ_2 as a free parameter and compute B_{t2}, $P_{\parallel 2}$ and A_2 as functions of r_s. In the analysis of Siewert and Fahr (2008) it is shown that including CGL invariance reduces the openness of the system. Indeed the downstream anisotropy is obtained as a function of the upstream anisotropy and the shock strength only which contrasts with the MHD expressions presented below.

The system (1)-(6) can be solved analytically in the parallel and perpendicular shock cases (Liu et al. 2007). For values of θ_{Bn} other than 0° and 90° we shall use a numerical method based on a Broyden's resolution scheme (Press et al. 1992). In the perpendicular shock case the downstream anisotropy may be expressed as

$$A_2 = \left[\beta_1 + 2M_{A1}^2\left(1 - \frac{1}{r_s}\right) + 1 - r_s^2\right] \times \left[\beta_1(5r_s - 4) + 2M_{A1}^2\left(r_s + \frac{3}{r_s} - 4\right) + 4(r_s - 1)\right]^{-1} \tag{8}$$

and in the parallel shock case :

$$A_2 = \left[\beta_1\left(\frac{3}{2}r_s - \frac{1}{2}\right) + M_{A1}^2(1 - r_s)\right] \times \left[\beta_1(2 - r_s) + 2M_{A1}^2\left(3 - r_s - \frac{2}{r_s}\right)\right]^{-1} \tag{9}$$

For simplicity isotropic solar wind conditions are assumed ($A_1 = 1$). Equation 8 above is equivalent to Equation 8 in Liu et al. (2007). On the contrary Equation 9 above differs from their Equation 10. We checked that solutions for downstream anisotropy computed independently 1/ from our Equation 9 and 2/ with our numerical method for $\theta_{Bn} = 0°$ are consistent (the anisotropy is a continuous function of θ_{Bn}). Accordingly the downstream anisotropy A_2 computed from our Equation 9 and displayed in the (M_{A1}, β_1) plane shows a different view from the one displayed in Figure 2 of Liu et al. (2007).

Finally, under the hypotheses of cold isotropic electrons and bi-Maxwellian plasma in the low frequency, long wavelength limit of the Vlasov-Maxwell equations, we define the mirror and firehose conditions by (Hall 1979; Hellinger 2007) :

$$C_M = \beta_\perp \left(\frac{T_\perp}{T_\parallel} - 1 \right) \tag{10}$$

$$C_F = \beta_\parallel \left(1 - \frac{T_\perp}{T_\parallel} \right) - 1 \tag{11}$$

According to these definitions the mirror and firehose instabilities occur for $C_M > 1$ and $C_F > 1$ respectively.

3. Anisotropy instabilities in the heliosheath

Our approach to determine heliosheath plasma conditions is the following. We use observations by the Voyager spacecraft and simulations to specify upstream parameters. RH relations are then solved in the (θ_{Bn}, r_s) plane in order to determine downstream parameters and corresponding values of C_M and C_F. Locations of the instability thresholds are thus obtained in the (θ_{Bn}, r_s) plane and compared to shock angle and strength effectively estimated for TS1 and TS3.

We shall discuss three types of shocks. First TS1, observed by V1 in inward motion, is considered (Liu et al. 2007); then simulated parameters for an outward motion of TS1 is studied (Whang et al. 2004). The shock parameters are distinctly different in the two situations : indeed an inward (outward) motion corresponds to periods of low (high) speed solar wind and strong (weak) shock. Finally TS3, observed by V2, is analyzed : it is a rather oblique shock contrary to TS1 which is almost perpendicular (Burlaga et al. 2008; Richardson et al. 2008). Parameter values are summarized in Table 1. Four other termination shock crossings are inferred from V2 observations : TS2, observed 3.7h before TS3, is close to TS1 (outward) observed by V1 as far as parameters are concerned, TS4 is only partially observed, and TS1 (here the first crossing by V2) and TS5 occurred during telemetry gaps.

In Figure 1 isocontours of C_M (solid line) and C_F (dash line) are plotted in the (θ_{Bn}, r_s) plane for TS1 in inward motion conditions (similarly in Figure 2 for TS1 in outward motion). The lines $C_M = 1$ and $C_F = 1$ represent the mirror and firehose instability thresholds respectively. The instability domain is below (above) this line for the mirror (firehose) instability. The contours $C_M = 0$ and $C_M = 3$ are discussed in the next section.

The firehose instability threshold is mostly independent of the shock angle θ_{Bn} and obtained for stronger shocks than the mirror instability. On the contrary the influence of the shock angle is not negligible for the mirror instability whose threshold occurs for weaker

shocks at large shock angles. This implies that the instability domain is larger for small θ_{Bn} (TS classes 1, 4 and 5 as shown in Figure 1).

V1 encountered an almost perpendicular shock ($\theta_{Bn} \simeq 86°$) in inward motion (Liu et al. 2007). For these conditions the shock strength was estimated to be $r_s = 3.0 \pm 0.2$ (Whang et al. 2004) and was later inferred to be $r_s = 2.6^{+0.4}_{-0.2}$ from the particle spectra (Stone et al. 2005). Therefore, from inspection of Figure 1 and by spanning the complete domain of strength values, the two instabilities may develop : for $2.4 < r_s < 3$ plasma conditions are mirror unstable (TS classes 4 and 5) whereas for $3.06 < r_s < 3.2$ (TS class 1) they are firehose unstable; the region $3 < r_s < 3.06$ is stable (TS classes 2 and 3). The situation studied in Liu et al. (2007) is showed by a cross in Figure 1 : we confirm that the plasma conditions are effectively mirror unstable ($C_M = 1.2$). Let us note that here we use the observed angle ($\theta_{Bn} = 86°$).

On the contrary, if the shock was in outward motion, the shock strength would be smaller, in the range $r_s = 2.5 \pm 0.2$ (Whang et al. 2004). Therefore, from inspection of Figure 2, it is obvious that plasma conditions could only be mirror unstable at whatever θ_{Bn} angles. We note that in both these situations (inward and outward motion), and for the range of parameters considered, the entropy $S = \frac{1}{2}k \ln(P_\perp^2 P_\parallel/\rho^5)$ increases across the shock in accordance with the second law of thermodynamics.

For upstream conditions observed ahead of TS3 (inward motion, figure not shown) the $C_M = 1$ contour variation is similar to those shown in Figures 1 and 2 and evolves from $r_s = 3.92$ for the parallel case to $r_s = 3.57$ for the perpendicular case. However TS3 is a very weak shock : $r_s \simeq 1.6 \pm 0.7$ (Richardson et al. 2008), and the entropy does not increase across it according to RH relations. Indeed for these upstream conditions the shock strength should be greater than 2.88 (in the exactly perpendicular case) for the entropy to increase (smaller values apply for decreasing angles). We checked that the more extreme values given in the estimation of Richardson et al. (2008) (largest $r_s = 2.3$ and smallest $\theta_{Bn} = 63°$) do not satisfy the entropy principle. One explanation may be that the particularly complex dynamics of shock reformation (actually observed by V2 (Burlaga et al. 2008)) invalidate the use of the static RH relations. Another explanation involves the computation of upstream parameters and the importance of pick-up ions. Indeed the temperature given in Table 1 for TS3 corresponds to the proton temperature only, whereas for TS1 a density-weighted average of the pick-up ion, solar wind wind proton and electron temperatures is used (Whang et al. 2004). The multi-fluid nature of the solar wind is adequately described by an effective Mach number including pick-up ion pressure (Fahr and Rucinski 1999). Similarly Richardson et al. (2008) explained that the heliosheath is effectively subsonic only if hot pick-up ions are considered when deriving wave properties.

4. Prediction on mirror associated magnetic structures

In this section we show that TS classes 3 ($0 < C_M < 1$), 4 ($1 < C_M < 3$) and 5 ($C_M > 3$) may be distinguishable with respect to the shapes of mirror associated structures potentially observed behind related shocks. Indeed recent studies combining observations in the Earth's magnetosheath, hybrid (particle) simulations and theory (Soucek et al. 2008; Califano et al. 2008; Génot et al. 2008b) have shown that the shape of mirror structures are very well correlated with the distance to threshold C_M. More specifically the skewness of the magnetic field amplitude distribution is negative (magnetic fluctuations look like holes) for $C_M < 1$ and is positive (magnetic fluctuations look like peaks) for $C_M \gtrsim 2$. Both kinds of structures were observed by V1 in the heliosheath (Burlaga et al. 2006). Sinusoidal or 'mixed' structures (vanishing skewness) are observed around $C_M \simeq 1.5$. It is interesting to note that holes structures are mostly observed for mirror stable conditions. This peculiar behaviour is inherent to a bistable phenomenon (Passot et al. 2006) which allows magnetic holes to survive stable conditions whereas magnetic peaks are damped. If we transpose these results to our TS classification, we could expect to observe magnetic holes behind TS class 3. These holes would have grown from mirror unstable conditions in a separate region and would have been convected back close to the TS where they could survive according to the bistability phenomenon. Behind TS classes 4 and 5 sinusoidal mirror structures and peaks are expected with a predilection for peaks in class 5. Recent observations of multiple shock crossings with V2 may validate this scenario which would illustrate the generality of astrophysical processes such as temperature anisotropy driven instabilities.

In planetary magnetosheaths it has been shown that the plasma β decreases from the shock to the magnetopause and is anti-correlated with the anisotropy (Fuselier et al. 1994), the plasma state remaining close to the mirror marginal stability. However in the heliosheath no similar trend has yet been detected. Conditions are probably much different in the upwind and downwind directions.

5. Summary

This paper presents a generic procedure to infer heliosheath plasma conditions with respect to temperature anisotropy instabilities downstream of the Termination Shock for arbitrary upstream parameters, shock angle and strength. We confront this both analytical and numerical approach with in-situ measurements recorded by the Voyager spacecraft. Different types of shocks have been crossed and heliosheath plasma behind these shocks may be stable or not with respect to the mirror and firehose instabilities. The procedure proposed here allows to take into account the measurement uncertainties of the shock angle and

strength in order to determine the actual downstream plasma state. The present calculation is also used to predict possible future observations in the heliosheath by comparison with the much covered Earth's bow shock and magnetosheath regions.

REFERENCES

Bavassano Cattaneo, M. B., C. Basile, G. Moreno, & J. D. Richardson 1998, J. Geophys. Res., 103, 11

Burlaga L. F., N. F. Ness, & M. H. Acũna 2006, Geophys. Res. Lett., 33, L21106, doi:10.1029/2006GL027276

Burlaga L. F., et al. 2008, Nature doi:10.1038/nature07029

Califano, F., P. Hellinger, E. Kuznetsov, T. Passot, P. L. Sulem, & P. Travnicek 2008, J. Geophys. Res., *in press*

Chao, J. K., Zhang, X. X., & Song, P. 1995, Geophys. Res. Lett., 22, 17

Erickson, G. M., Siscoe, G. L., Weimer, D. R., Siebert, K. D., Heinemann, M. A., Sonnerup, B. U.., Maynard, N. C., & White, W. W. 2002, Planetary and Space Science, Volume 50, Issue 5-6, 627

Fahr, H.-J., & D. Rucinski 1999, Astron. Astrophys., 350, 1071

Fahr, H.-J., & Siewert, M. 2007, Astrophysics and Space Sciences Transactions, 3, 21-27

Fuselier, S. A., B. J. Anderson, S. P. Gary, and R. E. Denton 1994, J. Geophys. Res., 14,93114,936, doi:10.1029/94JA00865.

V. Génot, E. Budnik, C. Jacquey, I. Dandouras, & E. Lucek 2008, Advances in Geosciences, *in press*

V. Génot, E. Budnik, P. Hellinger, T. Passot, G. Belmont, P. Trávníček, P.-L. Sulem, E. Lucek, & I. Dandouras, 2008, *submitted to Annales Geophysicae*

Hall, A. N. 1979, J. Plasma Phys., 21, 431

Hellinger P. 2007, Phys. Plasmas, 14, 8

Huddleston, D. E., R. J. Strangeway, X. Blanco-Cano, C. T. Russell, M. G. Kivelson, & K. K. Khurana 1999, J. Geophys. Res., 104, 10.1029/1999JA900195

Hudson, P. D. 1970, Planet. Space Sci., 18, 1611

Joy, S. P., Kivelson, M. G., Walker, R. J., Khurana, K. K., Russell, C. T., & Paterson, W. R. 2006, J. Geophys. Res., 111

Kasper J. C., A. J. Lazarus, & S. P. Gary 2002, Geophys. Res. Lett., 29, 1839, doi:10.1029/2002GL015128

Liu, Y., Richardson, J. D., Belcher, J. W., Kasper, J. C., & Skoug, R. M. 2006, J. Geophys. Res., 111

Liu, Y., Richardson, J. D., Belcher, J. W., & Kasper, J. C. 2007, ApJ, 659, L65

Passot T., V. Ruban, P. L. Sulem 2006, Phys. Plasmas, 13, 102310

Press, W. H., S.A. Teukolsky, W.T. Vetterling & B.P. Flannery 1992, Numerical Recipes in C: the art of scientific computing, Cambridge University Press

Richardson, J. D., Kasper, J. C., Wang, C., Belcher, J. W. & Lazarus, A. J. 2008, Nature doi:10.1038/nature07024

Russell, C. T., Riedler, W., Schwingenschuh, K., & Yeroshenko, Y. 1987, Geophys. Res. Lett., 14

Schekochihin, A. A., Cowley, S. C., Kulsrud, R. M., Rosin, M. S., & T. Heinemann 2008, Phys. Rev. Lett., 100, 081301

Siewert, M., & Fahr, H.-J. 2008, Astron. Astrophys., 485, 327-336

Soucek, J., E. Lucek, & I. Dandouras 2008, J. Geophys. Res., 113, A04203, doi:10.1029/2007JA012649

Stone, E. C., et al. 2005, Science, 309, 2017

Stone, E. C., et al. 2008, Nature doi:10.1038/nature07022

Vogl, D. F., Biernat, H. K., Erkaev, N. V., Farrugia, C. J., & Mhlbachler, S. 2001, Nonlin. Proc. Geophys., 8, 3

Whang, Y. C., L. F. Burlaga, Y.-M. Wang, & N. R. Sheeley Jr. 2004, Geophys. Res. Lett., 31, L03805, doi:10.1029/2003GL018679

Winterhalter, D., M. Neugebauer, B. E. Goldstein, E. J. Smith, S. J. Bame, & A. Balogh 1994, J. Geophys. Res., 99, 23

Upstream parameters	TS1 (inward motion)	TS1 (outward motion)	TS3 (inward motion)
Wind speed (km/s)	380	530	320
Density (cm^{-3})	8×10^{-4}	8×10^{-4}	0.001
Temperature (K)	5.4×10^{5}	12.2×10^{5}	10^{4}
Magnetic field (nT)	0.03	0.03	0.06
Anisotropy (A_1)	1	1	1
M_{A1}	16.3	22.7	7.6
β_1	32.8	77.4	0.19
Shock strength	3.0±0.2	2.5±0.2	1.58±0.71
Shock angle (°)	86	86	74.3±11.2

Table 1: Upstream parameters are from Liu et al. (2007) for TS1 (inward), from Whang et al. (2004) for TS1 (outward) and from Richardson et al. (2008) and Burlaga et al. (2008) for TS3.

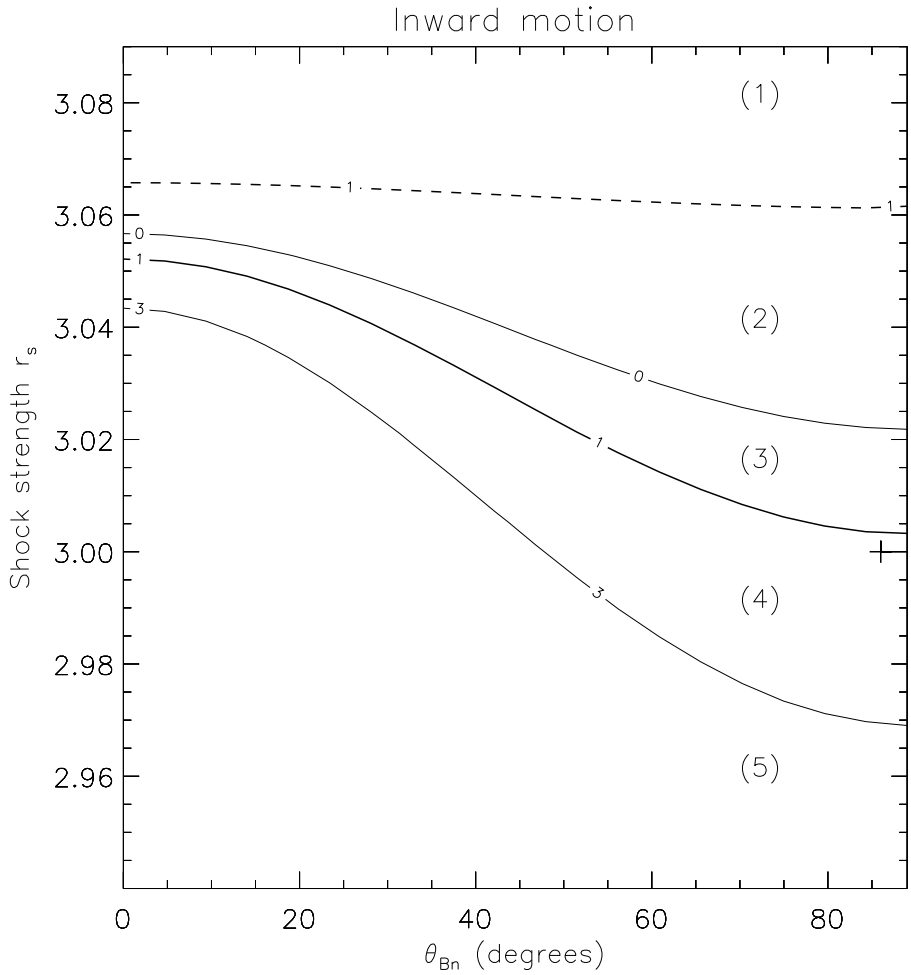

Fig. 1.— Mirror (solid thick line) and firehose (dash line) instability thresholds as a function of the shock angle θ_{Bn} and strength r_s for TS1 in inward motion conditions (see Table 1). These lines corresponds to $C_M = 1$ and $C_F = 1$ respectively (see text for definitions); the two thin lines correspond to $C_M = 0$ and $C_M = 3$. The heliosheath plasma is mirror (firehose) unstable for shock conditions below (above) the threshold line. Labeled regions corresponds to the five TS classes where the following processes may be observed : (1) firehose instability, (2) uniform stability, (3) possible existence of mirror stable magnetic hole structures, (4) mirror instability, (5) mirror instability with possible predominance of magnetic peak structures. The cross at $r_s = 3$ and $\theta = 86°$ corresponds to the TS conditions observed during V1 crossing ($C_M = 1.2$).

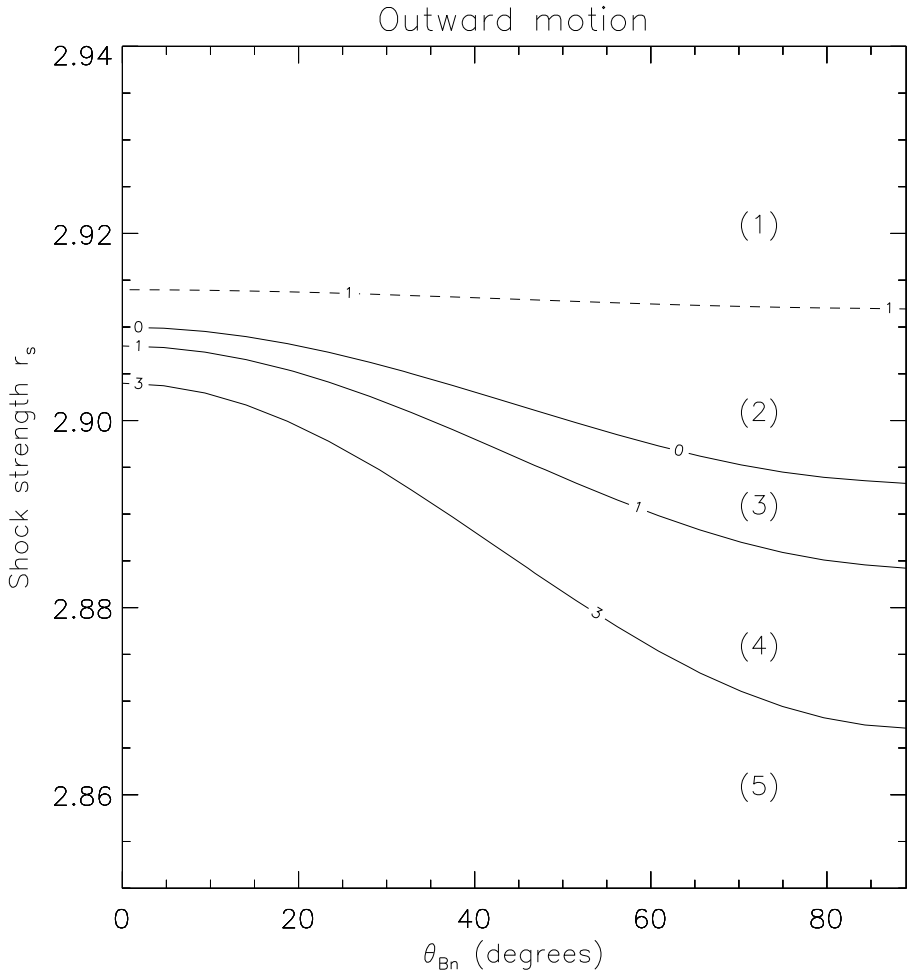

Fig. 2.— Same as Figure 1 for TS1 in outward motion conditions (see Table 1).